

## CIRCULAR POLARIZATION FROM STOCHASTIC SYNCHROTRON SOURCES

MATEUSZ RUSZKOWSKI AND MITCHELL C. BEGELMAN<sup>1</sup>  
 JILA, Campus Box 440, University of Colorado, Boulder CO 80309-0440  
 mr@jila.colorado.edu; mitch@quixote.colorado.edu

*To appear in ApJ*

## ABSTRACT

The transfer of polarized radiation in stochastic synchrotron sources is explored by means of analytic treatment and Monte Carlo simulations. We argue that the main mechanism responsible for the circular polarization properties of compact synchrotron sources is likely to be Faraday conversion and that, contrary to common expectation, a significant rate of Faraday rotation does not necessarily imply strong depolarization. The long-term persistence of the sign of circular polarization, observed in many sources, is most likely due to a small net magnetic flux generated in the central engine, carried along the jet axis and superimposed on a highly turbulent magnetic field. We show that the mean levels of circular and linear polarizations depend on the number of field reversals along the line of sight and that the gradient in Faraday rotation across turbulent regions can lead to “correlation depolarization”. Our model is potentially applicable to a wide range of synchrotron sources. In particular, we demonstrate how our model can naturally explain the excess of circular over linear polarization in the Galactic Center and the nearby spiral galaxy M81 and discuss its application to the quasar 3C 279, the intraday variable blazar PKS 1519-273 and the X-ray binary SS 433.

*Subject headings:* polarization: circular – stars: individual (SS433) – Galaxy: center – galaxies: individual (M81) – quasars: individual (3C 279) – BL Lacertae objects: individual PKS 1519-273

## 1. INTRODUCTION

Polarization has proven to be an important tool in AGN research. In principle, linear and particularly circular polarization observations of synchrotron radiation may permit measurements of various properties of jets such as: magnetic field strength and topology, the net magnetic flux carried by jets (and hence generated in the central engine), the energy spectrum of radiating particles, and the jet composition (i.e., whether jets are mainly composed of  $e^+ - e^-$  pairs or electron-proton plasma). The renewed interest in polarization of compact radio sources stems from two recent developments. First, Bower et al. (1999) detected circular polarization using the Very Large Array (VLA) in the best supermassive black hole candidate, the Galactic center (Sgr A\*). This discovery was quickly confirmed by Sault and Macquart (1999) using the Australia Telescope Compact Array (ATCA). Circular polarization was also detected in the celebrated X-ray binary system SS 433 (Fender et al. 2000). Moreover, the Very Long Baseline Array (VLBA) has now detected circular polarization in as many as 20 AGN (Wardle et al. 1998; Homan and Wardle 1999). Second, it is now possible to measure circular polarization with unprecedented accuracy of 0.01% using the ATCA (Rayner et al. 2000). This dramatic improvement in the observational status of polarization measurements has also brought new questions. For example, there is now growing observational evidence that the sign of circular polarization is persistent over decades (Komesaroff et al. 1984; Homan and Wardle 1999), which indicates that it is a fundamental property of jets. Another problem, which has not been satisfactorily explained as yet, is how to reconcile the high level of circular polar-

ization with the lower value of linear polarization in Sgr A\* (Bower et al. 1999) and M81\* (Brunthaler et al. 2001). Indeed, there is not even a general consensus on the mechanism responsible for the circular polarization properties of jets (Wardle et al. 1998).

In this paper we attempt to solve some of the theoretical puzzles. The paper is organized as follows. In the next section we summarize the most important observational facts. In Section 3 we briefly discuss mechanisms for producing circular polarization and argue that the most likely process is “Faraday conversion”. Section 4 presents our model for polarization and in the subsequent sections we compare Monte Carlo simulations with analytic results and discuss general implications for observations as well as specific observational cases. We summarize our conclusions in Section 7.

## 2. OBSERVATIONAL TRENDS

Compact radio sources typically show a linear polarization (LP) of a few percent of the total intensity (Jones et al. 1985). This is much less than the theoretical maximum for synchrotron sources, which can approach 70% in homogeneous sources with unidirectional magnetic field. Therefore, magnetic fields in radio sources are believed to be highly inhomogeneous, although the nonvanishing linear polarization is in itself an indirect indication of a certain degree of ordering of the field. Although the precise topology of the magnetic field in jets is not known, there are other compelling reasons, both theoretical and observational, to believe that magnetic fields are indeed partially ordered. On the observational side, these conclusions are based on measurements of the orientation of linear polar-

<sup>1</sup> Also at Department of Astrophysical and Planetary Sciences, University of Colorado

ization (**E** vector), which reveal coherent structures across jet images. This indicates that magnetic fields, which are predominantly perpendicular to the electric vectors, are also preferentially aligned, although in different sources or in different parts of the jet the magnetic fields can be mainly orthogonal (Wardle et al. 1998) or parallel (Jones et al. 1985; Rusk and Seaquist 1985) to the projected jet orientation. From the theoretical point of view, ordered jet magnetic field is expected when shocks compress an initially random field (Laing 1980, 1981; Marscher and Gear 1985; Hughes et al. 1989; Wardle and Roberts 1994) (**B** perpendicular to the jet axis) or when such initial fields are sheared to lie in a plane (Laing 1980, 1981; Begelman, Blandford and Rees 1984) (**B** parallel to the jet axis).

Circular polarization (CP) is a common feature of quasars and blazars (Rayner et al. 2000; Homan et al. 2001), is usually characterized by an approximately flat spectrum, and is generated near synchrotron self-absorbed jet cores (Homan and Wardle 1999). CP is detected in about 30%-50% of these objects. Measured degrees of CP are generally lower than the levels of linear polarization and usually range between 0.1 and 0.5% (Homan and Wardle 1999; Homan et al. 2001). As reported by Macquart et al. (2000) for the intraday variable source PKS 1519-273, the CP of variable components of intensity can be much higher than the overall circular polarization levels. Observations of proper motion of CP-producing regions in the quasar 3C 273 (Homan and Wardle 1999) suggest that circular polarization is intrinsic to the source, as opposed to being due to foreground effects. Most importantly, comparisons of CP measurements made within the last 30 years (Weiler and de Pater 1983; Komesaroff et al. 1984; Homan and Wardle 1999) with the most recent observations reveal that, despite CP variability, its sign is a persistent feature of AGN, which must therefore be related to a small net unidirectional component of magnetic field in jets.

### 3. MECHANISMS FOR PRODUCING CIRCULAR POLARIZATION

The most obvious candidate for explaining circular polarization of compact radio sources is intrinsic emission (Legg and Westfold 1968). Although intrinsic CP is roughly  $\pi_{c,int} \sim \gamma^{-1}$  where  $\gamma$  is the Lorentz factor of radiating electrons, in a realistic source it will most likely be strongly suppressed by the tangled magnetic field and possibly the emissivity from  $e^+ - e^-$  pairs, which do not contribute CP. Specifically,  $\pi_{c,int} \sim \gamma^{-1}(B_u/B_{rms})f_{pair} \ll 1\%$ , where  $B_u$  and  $B_{rms}$  are the unidirectional component of the magnetic field projected onto the line-of-sight and the fluctuating component of the field, respectively, and  $f_{pair} \equiv (n^- - n^+)/n^- + n^+ \leq 1$ . Therefore, intrinsic CP appears to be inadequate to explain the observed polarization. Other mechanisms have also been proposed, among which the most popular ones are coherent radiation processes (Benford and Tzach 2000), scintillation (Macquart and Melrose 2000) and Faraday conversion (Pacholczyk and Swihart 1975; Jones and O'Dell 1977a; Jones 1988; Wardle et al. 1998). The first of these mechanisms produces polarization in a narrow frequency range which now seems to be ruled out by multiband observations. The recently proposed scintillation mechanism, in which circular

polarization is stochastically produced by a birefringent screen located between the jet and the observer, fails to explain the persistent sign of circular polarization as the time-averaged CP signal is predicted to vanish. The last mechanism — Faraday conversion — seems to be the most promising one and in the next subsection we discuss it in more detail.

#### 3.1. Faraday rotation and conversion

The polarization of radiation changes as it propagates through any medium in which modes are characterized by different plasma speeds. In the case of cold plasma the modes are circularly polarized. The left and right circular modes have different phase velocities and therefore the linear polarization vector of the propagating radiation rotates. This effect is called Faraday rotation and it is often used to estimate magnetic field strength in the interstellar medium and to estimate pulsar distances. Note that Faraday rotation does not alter the degree of circular polarization, since any circular polarization can be decomposed into two independent linearly polarized waves. Faraday rotation is a specific example of a more general phenomenon called birefringence. In a medium whose natural modes are linearly or elliptically polarized, such as a plasma of relativistic particles, birefringence leads to the partial cyclic conversion between linearly and circularly polarized radiation as the phase relationships between the modes along the ray change with position. This effect is best visualized by means of the Poincaré sphere (Melrose and McPredhan 1991; Kennet and Melrose 1998). An arbitrary elliptical polarization can be represented by a vector **P** with its tip lying on the Poincaré sphere and characterized by Cartesian coordinates  $(Q, U, V)/I$ , where  $Q, U, V$  and  $I$  are the Stokes parameters (see Fig. 1). Thus, the north and south poles correspond to right and left circular polarizations and points on the equator to linear polarization. Different azimuthal positions on the sphere correspond to different orientations of the polarization ellipses. The polarization of natural modes of the medium is represented by a diagonal axis, whose polar angle measured from the vertical axis depends on whether the medium is dominated by cold ( $0^\circ$ ) or highly relativistic particles ( $90^\circ$ ). As the radiation passes through the medium, birefringence causes the tip of the polarization vector to rotate at a constant latitude around the axis of the natural plasma modes. In this picture, Faraday rotation corresponds to the case where the natural modes axis is vertical and the polarization vector **P** rotates around it. Note that, even if radiation initially has no circular polarization (i.e., **P** lies in the equatorial plane) and then encounters a medium in which the normal modes are elliptical, it will develop an elliptically polarized component. An interesting property of a relativistic birefringent plasma is that it can generate circular polarization even if it is composed almost entirely of electron-positron pairs. At first this may seem paradoxical, as one would expect electrons and positrons to contribute to CP with opposite signs. However, despite the fact that the intrinsic CP in such a case is indeed close to zero, some additional CP can be produced by conversion of linear polarization (Sazonov 1969; Noerdlinger 1978). In terms of the Poincaré sphere, this situation corresponds to the normal modes axis pointing close to but not exactly in the

equatorial plane. Therefore some conversion of intrinsic linear polarization may occur provided that there is some imbalance in the number of electrons and positrons.

### 3.1.1. Strong rotativity limit

Strong departures from mode circularity occur only when radiation propagates within a small angle  $\sim \nu_L/\nu$  of the direction perpendicular to the magnetic field, where  $\nu_L = eB/2\pi m_e c$ . Therefore radiative transfer is often performed in the quasi-longitudinal (QL) approximation. If the normal modes are highly elliptical then the opposite, quasi-transverse (QT), limit applies (Ginzburg 1961). In a typical observational situation it is usually assumed that Faraday rotation within the source cannot be too large, as this will lead to the suppression of linear polarization. However, this constraint does not prevent rotativity from achieving large values locally as long as the mean rotativity, i.e., averaged over all directions of magnetic field along the line of sight, is indeed relatively small. Such a situation may happen in a turbulent plasma. Some effects of turbulence on polarization were discussed by Jones (1988) who neglected a uniform magnetic field component and by Wardle et al. (1998), who presented results for the case of a small synchrotron depth. Technically, the strong rotativity regime is equivalent to the QL limit and in this paper we build our model on this approximation.

## 4. MODEL FOR POLARIZATION

We consider a highly tangled magnetic field with a very small mean component which is required to determine the sign of circular polarization. From a theoretical viewpoint, we would expect some net poloidal magnetic field, either originating from the central black hole or from the accretion disk, to be aligned preferentially along the jet axis. Specifically, from equipartition and flux freezing arguments applied to a conical jet (Blandford and Königl 1979) we get  $\langle B_{\parallel}^2 \rangle^{1/2} \sim \langle B_{\perp}^2 \rangle^{1/2} \sim B_{\text{rms}} \propto r^{-1}$  where  $r$  is the distance along the synchrotron emitting source and the symbols  $\parallel$  and  $\perp$  refer to magnetic fields parallel and perpendicular to the jet axis, respectively. From the flux-freezing argument applied to the small parallel bias in the magnetic field we obtain  $\langle B_{\perp} \rangle \sim 0$  and  $\langle B_{\parallel} \rangle \propto r^{-2} \propto \delta B_{\text{rms}}$ , where  $\delta \equiv B_u/B_{\text{rms}} \ll 1$  is the ratio of the uniform and fluctuating components of the magnetic field.

### 4.1. Mean Stokes parameters in the presence of field reversals

We solve the radiative transfer of polarized radiation in a turbulent plasma by adopting transfer equations for a piecewise homogeneous medium with a weakly anisotropic dielectric tensor (Sazonov 1969; Jones and O'Dell 1977a). Details of the transfer equations are given in the Appendix. We assume that the mean rotativity per unit synchrotron optical depth  $\langle \zeta_v^* \rangle \equiv \delta\zeta$  and that  $\langle \sin 2\phi \rangle = 0$  and  $\langle \cos 2\phi \rangle = 2p - 1$ , where  $0 \leq p \leq 1$  is a parameter describing the polarization direction and degree of order in the field. We also assume that circular absorptivity  $\zeta_v$  and circular emissivity  $\epsilon_v$  are both negligible.

#### 4.1.1. Large synchrotron depth limit

Averaging the transfer equations over orientations of the magnetic field, we obtain the following asymptotic expressions for large synchrotron optical depth:

$$\bar{I} + (2p - 1)\zeta_q \bar{Q} = J \quad (1)$$

$$\bar{Q} + \langle \zeta_v^* U \rangle + (2p - 1)\zeta_q \bar{I} = (2p - 1)\epsilon_q J \quad (2)$$

$$\bar{U} - \langle \zeta_v^* Q \rangle + (2p - 1)\bar{\zeta}_q^* \bar{V} = 0 \quad (3)$$

$$\bar{V} - (2p - 1)\bar{\zeta}_q^* \bar{U} = 0. \quad (4)$$

Note that  $\zeta_v^*$  is not statistically independent from  $U$  and  $Q$  due to the gradient in Faraday rotation across each cell. The correlation in eq. (2) then reads:

$$\langle \zeta_v^* U \rangle = \delta\zeta \bar{U} + \langle \tilde{\zeta}_v^* \tilde{U} \rangle, \quad (5)$$

where  $\tilde{\zeta}_v^*$  and  $\tilde{U}$  denotes the fluctuating part of  $\zeta_v^*$  and  $U$ . An analogous relation holds for  $Q$  in eq. (3). We neglect the term  $\langle \tilde{\zeta}_q^* \tilde{U} \rangle$  in eq. (4) as convertibility is a much weaker function of plasma parameters than rotativity. It will be shown in Section 4.1.3 that the correlations  $\langle \tilde{\zeta}_v^* \tilde{U} \rangle$  and  $\langle \tilde{\zeta}_v^* \tilde{Q} \rangle$  tend to zero as the number of field reversals along the line of sight increases and that

$$-\langle \tilde{\zeta}_v^* \tilde{Q} \rangle / \bar{U} = \langle \tilde{\zeta}_v^* \tilde{U} \rangle / \bar{Q} \equiv \xi. \quad (6)$$

This implies that the mean levels of circular and linear polarizations will also depend on the number of the field reversals along the line of sight. Setting  $\bar{\pi}_q = \bar{Q}/\bar{I}$ ,  $\bar{\pi}_u = \bar{U}/\bar{I}$  and  $\bar{\pi}_v = \bar{V}/\bar{I}$ , we get mean normalized Stokes parameters from equations (1)–(4):

$$\bar{\pi}_q = \frac{(2p - 1)[1 - \xi + (2p - 1)^2 \bar{\zeta}_q^{*2}](\epsilon_q - \zeta_q)}{\mathcal{D}} \quad (7)$$

$$\bar{\pi}_u = \frac{(2p - 1)\delta\zeta(\epsilon_q - \zeta_q)}{\mathcal{D}} \quad (8)$$

$$\bar{\pi}_v = \frac{(2p - 1)^2 \bar{\zeta}_q^{*2} \delta\zeta(\epsilon_q - \zeta_q)}{\mathcal{D}}, \quad (9)$$

where

$$\mathcal{D} \equiv 1 + 2\xi + (2p - 1)^2(\zeta_q^{*2} - \zeta_q \epsilon_q) + \delta^2 \zeta^2 + [\xi - (2p - 1)^2 \zeta_q \epsilon_q][\xi + (2p - 1)^2 \bar{\zeta}_q^{*2}], \quad (10)$$

Note that

$$\frac{\bar{\pi}_v}{\bar{\pi}_u} = (2p - 1)\bar{\zeta}_q^* \quad (11)$$

$$\frac{\bar{\pi}_v}{\bar{\pi}_q} = \frac{(2p - 1)\bar{\zeta}_q^* \delta\zeta}{1 + \xi + (2p - 1)^2 \bar{\zeta}_q^{*2}}. \quad (12)$$

Therefore, circular polarization  $\bar{\pi}_c = -\bar{\pi}_v$  can dominate over linear polarization  $\bar{\pi}_l = (\bar{\pi}_q^2 + \bar{\pi}_u^2)^{1/2}$  if  $\delta\zeta \gtrsim (2p - 1)\bar{\zeta}_q^* > 1$ , where the last inequality holds for a large number of field reversals along the line of sight.

#### 4.1.2. Small synchrotron depth limit

In the limit of small synchrotron depth and for  $\delta\zeta \gtrsim 1$ , we approximately have:

$$\frac{d\bar{I}}{d\tau} = J \quad (13)$$

$$\frac{d\bar{Q}}{d\tau} + \delta\zeta\bar{U} + \langle\tilde{\zeta}_v^*\tilde{U}\rangle = (2p-1)\epsilon_q J \quad (14)$$

$$\frac{d\bar{U}}{d\tau} - \delta\zeta\bar{Q} - \langle\tilde{\zeta}_v^*\tilde{Q}\rangle = 0 \quad (15)$$

$$\frac{d\bar{V}}{d\tau} - (2p-1)\bar{\zeta}_q^*\bar{U} = 0. \quad (16)$$

Introducing  $X \equiv \bar{Q} + i\bar{U}$ , where  $i = \sqrt{-1}$ , we obtain:

$$\frac{dX}{d\tau} + (\xi - i\delta\zeta)X = (2p-1)\epsilon_q J \quad (17)$$

Solving eq. (16) and using eq. (17) we get:

$$\bar{\pi}_l = (2p-1)\epsilon_q \left[ \frac{1 - 2e^{-\tau_\xi} \cos \tau_r + e^{-2\tau_\xi}}{\tau_\xi^2 + \tau_r^2} \right]^{1/2} \quad (18)$$

$$\bar{\pi}_v = (2p-1)^2 \epsilon_q \frac{\tau_c}{\tau_\xi^2 + \tau_r^2} \times \left[ \tau_r + \frac{[2\tau_r\tau_\xi \cos \tau_r + (\tau_\xi^2 - \tau_r^2) \sin \tau_r]e^{-\tau_\xi} - 2\tau_r\tau_\xi}{\tau_\xi^2 + \tau_r^2} \right]^{1/2} \quad (19)$$

where  $\tau_r = \delta\zeta\tau$ ,  $\tau_c = \zeta_q^*\tau$  and  $\tau_\xi = \xi\tau$  are the rotation, conversion and ‘correlation’ depths, respectively. As in the synchrotron thick case, circular polarization can exceed linear polarization. For example, when  $\tau_\xi$  is negligible, the CP/LP ratio exceeds unity if:

$$(2p-1)\tau_c \gtrsim 2 \left| \sin \left( \frac{\tau_r}{2} \right) \right|. \quad (20)$$

As equations (6)–(9) for the synchrotron thick case and equations (18) and (19) for the synchrotron thin case clearly demonstrate, correlations induced by the gradient in Faraday rotation across turbulent regions have a depolarizing effect on linear and circular polarizations.

#### 4.1.3. Effect of statistical fluctuations on the mean Stokes parameters

Having obtained averaged quantities, we now proceed to calculate the effect of statistical fluctuations on the mean Stokes parameters. We introduce the following notation for the mean and fluctuating parts of the Stokes parameters:  $S = \bar{S} + \tilde{S}$ , where  $\langle\tilde{S}_i\rangle = 0$ ; and for the angular distribution of the projected magnetic field:  $\sin 2\phi \equiv a$ ,  $\cos 2\phi = (2p-1) + b$ , where  $\langle a \rangle = \langle b \rangle = \langle ab \rangle = 0$ . We write the fluctuating rotativity as  $\tilde{\zeta}_v^* \equiv \delta\zeta + \tilde{\zeta}$ , where  $\langle\tilde{\zeta}\rangle = 0$  but  $\tilde{\zeta} \sim \mathcal{O}(\zeta)$ . We constrain ourselves to the case dominated by Faraday rotation, i.e., we have  $|\zeta Q| \gg |a\zeta_q I|$ , etc. In such a case, the lowest order terms do not depend on the fluctuations in the orientation of the projected magnetic field  $\phi$ . Thus, retaining only leading terms, we obtain the fluctuating part of the transfer equations for  $\tilde{Q}$  and  $\tilde{U}$ :

$$\frac{d\tilde{Q}}{d\tau} + \tilde{\zeta}(\bar{U} + \tilde{U}) = 0 \quad (21)$$

$$\frac{d\tilde{U}}{d\tau} - \tilde{\zeta}(\bar{Q} + \tilde{Q}) = 0. \quad (22)$$

Note that when the fluctuations in  $Q$  and  $U$  are not dominated by rotativity terms, they are determined by variations in the orientation of the magnetic field. From equations (21) and (22) we can obtain corrections to the mean Stokes parameters due to the gradient in Faraday rotation across each cell:

$$\langle\tilde{\zeta}_v^*\tilde{Q}\rangle = - \left\langle \frac{\Delta\tau}{2} \tilde{\zeta}^2 (\bar{U} + \tilde{U}) \right\rangle = -\frac{1}{2}\bar{U}\langle\tilde{\zeta}^2\Delta\tau\rangle \quad (23)$$

$$\langle\tilde{\zeta}_v^*\tilde{U}\rangle = \frac{1}{2}\bar{Q}\langle\tilde{\zeta}^2\Delta\tau\rangle, \quad (24)$$

where  $\Delta\tau = \Delta\tau(\sin\theta)^{\alpha+3/2}$ ,  $\theta$  is the angle between the line of sight and the direction of the magnetic field,  $\Delta\tau = \tau_o/N$ ,  $\tau_o$  is the maximum synchrotron depth and  $N$  is the number of turbulent zones along the line of sight within this depth. Although these terms play an important role in the expressions for the mean Stokes parameters (equations [6]–[10] and [18]–[19]), they introduce only higher order corrections  $\sim \mathcal{O}(\zeta^2\Delta\tau/2)$  to the fluctuation equations and therefore should not be taken into account in equations (21) and (22) for the treatment to be self-consistent (recall that we assume that  $\zeta\Delta\tau < 1$ ). Note also that both  $\langle\tilde{\zeta}_v^*\tilde{Q}\rangle$  and  $\langle\tilde{\zeta}_v^*\tilde{U}\rangle$  are proportional to  $\tau_o N^{-1}$  and therefore asymptotically tend to zero as the number of field reversals along the line of sight increases.

We note that the presence of inhomogeneities in the magnetic field can, under certain circumstances, introduce additional complications into the radiative transfer due to the tracking and coupling of plasma modes. As the propagating wave goes from the QL to the QT regime (i.e.  $\mathbf{B}$  almost perpendicular to the line of sight) and then back to the QL regime, it can adiabatically adjust itself to the shifting nature of the eigenmodes provided that  $\zeta_{ov}\Delta\tau \gg 1$ , where  $\zeta_{ov} \equiv \zeta_\alpha^{*v}\gamma^2 \ln \gamma_i / \gamma_i^3$  (Björnsson 1990; Thompson et al. 1994; Fukui et al. 1998), i.e., provided that the gradient in the magnetic field is sufficiently small. In the opposite limit, the propagating wave does not ‘notice’ any inhomogeneities. In such a case, a circularly polarized wave will preserve its helicity as it crosses the QT region. Therefore, our assumption that Stokes  $I$ ,  $Q$ ,  $U$  and, in particular,  $V$ , are continuous at sharp boundaries between the turbulent cells, is consistent with our initial assumption that  $\zeta_{ov}\Delta\tau < 1$ . A spatially varying magnetic field can also introduce mode coupling when the coupling constant  $\mathcal{L} \sim \zeta_{ov}/(\zeta_\alpha^2\Delta\tau) \sim 1$ , where  $\zeta_{ov} \equiv 2\zeta_\alpha^{*q} \ln(\gamma/\gamma_i)$  (Jones and O’Dell 1977b) even in the QL region (i.e.,  $\mathbf{B}$  not in a direction almost perpendicular to the line of sight). When  $\mathcal{L} \ll 1$  and propagation occurs in the QL regime, coupling effects are unimportant. In the opposite limit when  $\mathcal{L} \gg 1$ , and when there is no uniform component of the magnetic field, radiation propagates as in a vacuum. Although we present no formal proof, we argue that in the latter limit radiation will be unaffected by the fluctuating component of the magnetic field and will be sensitive only to the mean bias component of the total magnetic field. In a real situation, the precise value of  $\mathcal{L}$  will depend on the details of magnetohydrodynamical turbulence. However, since our calculations were performed assuming a piece-wise homogeneous medium, technically our results

are exact. This is consistent with claims made by Jones (1988), who also considered the piece-wise homogeneous case and performed calculations using “standard” transfer equations and the wave equation. He obtained practically identical results from the two methods even though some of his results formally violated the non-coupling criterion. In a real situation we would expect some gradient of magnetic field across each turbulent cell but, again, in general the results will depend on the detailed treatment of the MHD turbulence which is beyond the scope of this work.

## 5. RESULTS AND IMPLICATIONS

We now consider a range of specific examples aimed at demonstrating predictions of our model and the consistency of our formulae with the results of Monte Carlo simulations. As mentioned in Section 3.1.1, we focus on cases where Faraday rotation per unit synchrotron optical depth  $\zeta_v^*$  is large. Specifically, we assume that the typical mean Lorentz factor of radiating electrons  $\gamma \sim 10^2$  and that the electron energy distribution function has a power-law form  $n(\gamma) \propto \gamma^{-(2\alpha+1)}$ , where  $\alpha$  is the spectral index of optically thin synchrotron emission. We use  $\alpha = 0.5$  and assume that the electron distribution is cut-off below  $\gamma_i \sim$  a few. For example, for the maximum brightness temperature  $T_b \sim 10^{11} K$  (Readhead 1994) we have  $\gamma \sim 3kT_b/m_ec^2 \sim 50$ , which corresponds to mean rotation and conversion per unit synchrotron optical depth of order  $\sim \delta\zeta_v^* \sim 3 \times 10^3 \delta \ln \gamma_i / \gamma_i^3$  and  $\zeta_q^* \sim -\ln(\gamma/\gamma_i)$ , respectively, for  $\nu \sim \gamma^2 eB/2\pi m_ec^2$ . In order to facilitate comparison of analytical and numerical results we use appropriate synchrotron depth-weighted solid angle averages of coefficients of rotativity  $\zeta_v^*$  and convertibility  $\zeta_q^*$  which include the effect of inclination of the uniform component of magnetic field to the line of sight:

$$\bar{\zeta}_{q,v}^* = \frac{\langle \zeta_{q,v}^* (B \sin \theta)^{\alpha+3/2} \rangle_\Omega}{\langle (B \sin \theta)^{\alpha+3/2} \rangle_\Omega}. \quad (25)$$

Retaining only the leading terms, we get

$$\bar{\zeta}_q^* = -2\zeta_\alpha^{*q} \ln\left(\frac{\gamma}{\gamma_i}\right) + \frac{3}{8}\pi\left(\frac{1}{2} - \ln 2\right)\zeta_\alpha^{*q} \quad (26)$$

$$\bar{\zeta}_v^* = \frac{3}{2}\zeta_\alpha^{*v}\gamma^2 \frac{\ln \gamma_i}{\gamma_i^3} \delta \cos \theta_u, \quad (27)$$

where  $\theta_u$  is the angle between the line of sight and the direction of the uniform magnetic field component. Analogously, for the correlation terms (equations [23] and [24]), we use

$$-\frac{\langle \tilde{\zeta}_v^* \tilde{Q} \rangle}{\bar{U}} = \frac{\langle \tilde{\zeta}_v^* \tilde{U} \rangle}{\bar{Q}} = \frac{\Delta\tau}{4} \left( \zeta_\alpha^{*v} \gamma^2 \frac{\ln \gamma_i}{\gamma_i^3} \right)^2 \equiv \xi. \quad (28)$$

### 5.1. Mean linear and circular polarizations

Fig. 2 presents mean linear (upper panel) and circular polarizations for the case of radiation transfer through a high synchrotron depth. The uppermost lines on each panel show analytic results for “saturated” polarizations corresponding to  $\xi \lesssim 1$  for  $p = 1$  (i.e., no dispersion of the projected magnetic field on the sky), and filled squares connected by dashed lines denote results of numerical simulations. Small systematic differences on Figures 2 and 3

<sup>2</sup> We further comment on the choice of parameters and consider more general situations while discussing specific observational cases in Sections 6.1 and 6.2

between the analytical curves and the numerical ones at higher values of  $\delta$  are due to the fact that the analytical formulae do not include higher order  $\delta$ -terms. The general behavior of these curves can be understood in simple terms. Linear polarization gradually decreases with  $\delta$  (and mean rotativity  $\bar{\zeta}_v^*$ ) as a result of the increasing strength of Faraday depolarization. Note that, contrary to common expectation, the mean linear polarization does not vanish as the result of a highly inhomogeneous magnetic field even though the magnitude of rotation per unit synchrotron optical depth is very large. As expected, circular polarization initially becomes stronger with an increasing component of the uniform magnetic field parallel to the line-of-sight. However, as Faraday depolarization gradually eliminates linear polarization (both Stokes  $Q$  and  $U$  are affected by this process), there is a reduced amount of  $U$  available for conversion into circular polarization (Stokes  $V$ ). Thus circular polarization has an extremum.

Other curves on Fig. 2 represent the case of “unsaturated” polarization when  $\xi \gtrsim 1$ . In such situations, the levels of both linear and circular polarizations systematically decline as  $N$  decreases. Note that the number of turbulent zones along the line of sight cannot be arbitrarily low, as this would reduce the mean polarization levels to very low values due to the increasing influence of the correlations between rotativity and Stokes  $Q$  and  $U$  parameters. Apart from affecting the mean polarization levels, increasing the number of field reversals along the line of sight also reduces the polarization fluctuations. Due to the finite size of the telescope beam, the fluctuations are further suppressed, however the beam averaging process does not affect the mean level of circular polarization. It also does not influence the mean level of linear polarization, provided that LP fluctuations are not very large prior to the beam averaging. Assuming that the number of turbulent zones in each of the perpendicular directions across the telescope beam is very roughly comparable to  $N$ , we conclude that fluctuations in the mean levels of CP and LP due to the stochastic nature of the plasma should be relatively small. Indeed, even though our numerical results for the mean circular and linear polarizations were obtained for a number of “pencil beams” much smaller than  $N^2$ , none of our results exhibit strong fluctuations. Thus, by demanding that there be enough turbulent cells along the line of sight to avoid correlation depolarization, we also guarantee that the polarization variability should be dominated by changes in the mean plasma parameters (e.g., the magnitude of the uniform component of the magnetic field, dispersion of the projected random magnetic field on the sky, the synchrotron depth, etc.), rather than by statistical fluctuations in, e.g., the orientation of the local turbulent magnetic field. This also assures that the sign of circular polarization should be a persistent feature — variations of the mean plasma parameters are not likely to change the sense of circular polarization, provided that the synchrotron optical depth does not change dramatically from low to very high values (see below) and the orientation of the mean field remains the same.

Fig. 3 illustrates the effect of relaxing the assumption of

that the projected magnetic field has zero dispersion on the sky. As the projected orientation of the magnetic field becomes increasingly chaotic ( $p \rightarrow 0.5$ ), the magnitudes of linear and circular polarizations gradually decline.

As both Figures 2 and 3 indicate, circular polarization can exceed linear polarization at higher values of the bias parameter  $\delta$ . The excess of CP over LP requires significant Faraday depolarization of linear polarization. Nevertheless, even a small amount of  $U$  can then be effectively converted to circular polarization, leading to CP/LP ratios in excess of unity. It is even conceivable to have a situation in which linear polarization falls below the detection threshold whereas circular polarization is still easily observable. Note that significant Faraday depolarization does not require a large bias  $\delta$  (i.e., exceeding unity) because of the large values of rotativity. This is consistent with observations which do not reveal any dominant large scale unidirectional fields. Such fields would lead to very strong linear polarization and are also unexpected on theoretical grounds.

In real sources the effective synchrotron optical depth will depend not only on the emission properties of the plasma along the line of sight but also, among other factors, on the solid angle subtended by the emitting region. In a realistic situation, the telescope will integrate over a finite-size beam with different synchrotron depths along different lines of sight. Thus, the emission from the synchrotron self-absorbed core of a jet will be weighted by a smaller solid angle than the emission from the more extended regions which have lower synchrotron depths and, therefore, lower surface brightness. Detailed calculations of the polarization properties of specific jet models are beyond the scope of this paper and will be presented in a forthcoming publication (Ruszkowski and Begelman, in preparation). Fig. 4 illustrates the effect of varying the total synchrotron depth  $\tau_o$  for ‘saturated’ polarization ( $\xi \lesssim 1$ ). For large  $\tau_o$  the results are similar to the ones presented on Fig. 2 and 3. In the opposite extreme, i.e., when  $\tau_o$  tends to zero, we have qualitatively similar behavior with the main difference being that the helicity of circular polarization is reversed. As in the high synchrotron depth case, the general trends in the polarization behavior can be understood in simple terms. The gradual decline of linear polarization with  $\delta$  is just a result of Faraday depolarization. As radiation propagates through the plasma, Stokes  $U$  is generated from Stokes  $Q$  due to Faraday rotation. Therefore, circular polarization, which is produced from Stokes  $U$  by Faraday conversion, initially increases. However, for large  $\delta$ , Faraday depolarization reduces Stokes  $Q$  and  $U$  and thus leads to the suppression of circular polarization. The oscillations in linear and circular polarizations are due to cyclic rotation of Stokes  $Q$  into  $U$  followed by conversion to  $V$ . Note that, for a narrow range of intermediate values of synchrotron depth, the behavior of CP resembles that of low  $\tau_o$  when  $\delta$  (and the mean rotativity) is small, and that of high  $\tau_o$  when  $\delta$  is larger.

The effects of ‘correlation depolarization’ for synchrotron depths around unity are shown in Fig. 5. This figure also demonstrates our analytic results for small synchrotron depths (dashed lines). Clearly, our analytic solutions for both very large and small synchrotron depths

adequately describe the numerical results which smoothly join the two regimes.

## 6. APPLICATION TO SPECIFIC SOURCES

### 6.1. *The case of quasar 3C279*

Wardle et al. (1998) reported the discovery of circular and linear polarization in 3C 279 and attributed CP to internal Faraday conversion. Typical fractional linear and circular polarizations in 3C 279 are of order  $\sim 10\%$  and  $\lesssim 1\%$ , respectively. Wardle et al. (1998) concluded that if the jet is composed of normal plasma, then the low-energy cut-off of the energy distribution of relativistic electrons must be as high as  $\gamma_i \sim 100$  in order to avoid Faraday depolarization and overproduction of the jet kinetic power. They considered synchrotron thin models with a bias in magnetic field and a small number of field reversals along the line of sight but neglected the dispersion of the projected magnetic field on the sky. They were unable to fit their polarization models to the observational data for  $\gamma_i \gtrsim 20$  and thus claimed that the jet must be pair-dominated. However, the above observational constraints on CP and LP and the jet energetics can be satisfied for a variety of microscopic plasma parameters. This is due to the fact that different ‘microscopic’ parameters, such as  $\gamma_i$ , the ratio of the cold to relativistic electron number densities, or the positron fraction, can lead to similar ‘macroscopic’ parameters such as convertibility and rotativity. In order to illustrate this, we consider two radically different examples and show that both cases can lead to the same CP and LP.

#### 6.1.1. *Electron-proton jet*

In this example, plasma is composed exclusively of a mixture of protons and electrons with both relativistic and cold populations being present. For instance, for a low-energy cut-off  $\gamma_i \sim 30$  and an electron number density-weighted mean Lorentz factor  $\gamma \sim 50$ , we get  $\langle \zeta_v^* \rangle \sim 80(n_c/n_r)\delta$  and  $\langle \zeta_q^* \rangle \sim -0.5$  (for  $n_c/n_r \ll 10^2$ ; see Appendix for details). The above value of rest-frame  $\gamma$  is consistent with self-absorbed sources having brightness temperatures in a narrow range close to  $\sim 10^{11} K$  (Readhead 1994). The actual energy distribution of the radiating particles will not be characterized by sharp energy cut-offs but will rather be a smooth function (Shimada and Hoshino 2000; Dieckmann et al. 2000). However, the detailed treatment of these subtleties is beyond the scope of this paper and we believe that the overall complexity of the problem justifies the use of our approximate treatment. For the above choice of parameters, the main contribution to rotativity comes from cold electrons as long as  $n_c/n_r \gtrsim 5 \times 10^{-3}$  (cf. eq. [A9]). The required levels of LP and CP can be obtained, for example, when  $p = 1$  and the combination  $(n_c/n_r)\delta \sim 2.5 \times 10^{-3}$ , as this assures sufficiently low mean rotativity that it does not lead to Faraday depolarization. Bear in mind that the admixture of cold electrons does not have to be large to explain the data. For example, we get the right levels of LP and CP for  $n_c/n_r \sim 5 \times 10^{-2}$  and  $\delta \sim 5 \times 10^{-2}$ . Interestingly, a jet with such a plasma composition could carry roughly as small a kinetic power as the pure electron-positron jet with the same emissivity, since the ratio of kinetic powers of an  $e$ - $p$  jet to a pure relativistic  $e^+e^-$

jet is  $\sim 18.4(\langle\gamma\rangle_{e^+e^-}/50)^{-1}(\gamma_{i,e^+e^-}/\gamma_{i,pe})$ , where we have assumed that protons are cold and have used  $\alpha = 0.5$  and where  $e^+e^-$  and  $pe$  refer to pair plasma and normal plasma, respectively. This means that, in principle, one can also explain the mean levels of circular and linear polarizations in 3C 279 for much lower values of  $\gamma_i$  than the one used above and therefore much higher rotativity, provided that the bias parameter  $\delta$  is also much lower. For example, the right levels of CP and LP can be obtained for  $\gamma_i = 3$ ,  $\gamma = 50$ ,  $N = 1875$ ,  $\delta \sim 3 \times 10^{-3}$  and  $\tau = 1$  (see middle panels in Fig. 5). We note that observational constraints on jet composition based on energetics should be taken with caution in any case, as kinetic luminosities derived from these methods scale with high powers of poorly determined observational quantities.

### 6.1.2. Electron-positron jet

The alternative possibility is that the jet is dominated by relativistic pair plasma. For example, for  $\gamma_i = 2$  and  $\gamma = 50$  we get  $\langle\zeta_q^*\rangle \sim -3.1$  and  $\langle\zeta_v^*\rangle \sim 1.4 \times 10^2 \delta (n_p/n_e)$ , where  $n_p$  and  $n_e$  are the number densities of protons and electrons, respectively. Agreement with the observed fractional linear and circular polarizations can be obtained for  $p = 1$  and  $(n_p/n_e)\delta \sim 2.1 \times 10^{-3}$ . Depending on the actual values of  $\delta$  and the ratio of protons to electrons, the jet may be pair-dominated in the sense that  $n_e \gg n_p$  while being dominated dynamically by protons; or it can be dominated by pairs both numberwise and dynamically. Recent theoretical work of Sikora and Madejski (2000) suggests that jets may be pair-dominated numberwise but still dynamically dominated by protons.

## 6.2. The case of Sgr A\*

Among the most intriguing sets of polarization observations are those of the Galactic center. Observations of stellar proper motions in the vicinity of the nonthermal source in the center of the Galaxy (Sgr A\*) reveal the presence of a  $\sim 2.6 \times 10^6 M_\odot$  compact object — the most convincing candidate for a supermassive black hole (Eckart and Genzel 1996, 1997; Ghez et al. 1998). Recently Bower et al. (1999) reported the detection of circular polarization from Sgr A\* with the VLA, which was confirmed by Sault and Macquart (1999) using ATCA. The typical level of CP in their observations was  $\sim 0.3\%$ , greater than the level of linear polarization. This result may seem surprising in light of the strong limits on the ratio of CP to LP in AGN where CP/LP is usually much less than unity (Weiler and de Pater 1983). However, as explained above, an excess of CP over LP can be explained easily in the framework of our model. Archival VLA data indicate that the mean CP was stable over ten years (Bower 2000). This is also not surprising as our model naturally predicts a persistent CP sign provided that the number of field reversals, either along one line-of-sight or across the beam area, is sufficiently large and the source does not undergo dramatic changes from synchrotron thin to synchrotron thick regimes. However, short-term circular polarization variability ( $\sim$  a few days) is also present. Interestingly, recent VLA observations from 1.4 to 15 GHz separated by a week revealed a CP increase at frequencies greater than 5 GHz, which coincided with an increase in the total intensity (Bower et al. 2000). The CP spectrum was

characterized by a flat to slightly positive spectral index ( $\pi_c \propto \nu^\beta$ ,  $\beta \gtrsim 0$ ). This result can also be accounted for in our model. For example, in the framework of a self-absorbed, self-similar jet model (Blandford and Königl 1979) but with a small bias  $\delta$  we have  $\langle\zeta_v^*\rangle \propto \delta \propto B \propto \nu$ . Assuming that  $\xi \gtrsim \epsilon_q \zeta_q$  and  $q \equiv (2p - 1)^2 \langle\zeta_q^*\rangle^2 \gg 1$ , and then demanding  $|\pi_c|/\pi_l \gtrsim 1$  and  $\beta \gtrsim 0$ , we obtain the following criterion which leads to the observed behavior (cf. eq. [7]–[10]):

$$(\xi + q)^2 q^{-1} \lesssim (\delta \zeta)^2 \lesssim 2\xi + q + \xi(\xi + q). \quad (29)$$

For instance, for  $\xi = 20$ ,  $\langle\zeta_q^*\rangle \sim -10$ ,  $\delta \zeta \sim 40$  and  $p = 1$  we have  $\beta \gtrsim 0$ ,  $|\pi_c|/\pi_l \sim 3$  and  $|\pi_c| \sim 0.6\%$ . Such values of the mean convertibility and rotativity could be obtained in the case of predominantly cold  $e^-p$  plasma with a small admixture of relativistic electrons. Note, however, that a certain amount of relativistic particles is always essential as synchrotron processes dominate emission and absorption in typical nonthermal sources. Specifically, the minimum and maximum size of Sgr A\* constrain the brightness temperature to be  $10^{10} \lesssim T_b \lesssim 5 \times 10^{11} K$  (Melia and Falcke 2001), which is within the range of typical AGN radio cores. Taking  $T_b \sim 10^{11}$  as the representative rest frame value (Readhead 1994), we get  $\gamma \sim 50$ . For minimum cut-off Lorentz factor  $\gamma_i = 2$ , this gives relativistic contributions to convertibility and rotativity equal to  $\langle\zeta_q^{*(r)}\rangle \sim -3$  and  $\langle\zeta_v^{*(r)}\rangle \sim 275\delta$ , respectively. Provided that dielectric suppression (Razin effect) is unimportant, the overall transfer coefficients are merely the sums of cold ( $c$ ) and relativistic ( $r$ ) contributions. Thus, for  $\zeta_v^{*(c)}/\zeta_v^{*(r)} \sim 4.3(n_c/n_r)$  and  $\zeta_q^{*(c)}/\zeta_q^{*(r)} \sim 0.08(n_c/n_r)$  (see Appendix), we obtain  $(n_c/n_r) \sim 30$  and  $\delta \sim 10^{-3}$ , which corresponds to the required values of the mean convertibility and rotativity.

It has recently been suggested that observations of linear polarization can be used to constrain the accretion rate in Sgr A\* and other low-luminosity AGN (Agol 2000; Quataert and Gruzinov 2000). These authors base their argument on the assumption that the Faraday rotation measure has to be sufficiently small in order not to suppress strong linear polarization (Aitken et al. 2000). This assumption places limits on density and magnetic field strength and leads to very low accretion rates  $\sim 10^{-8}$  to  $10^{-9} M_\odot \text{ yr}^{-1}$ . As noted by Agol (2000) and Quataert and Gruzinov (2000), this is inconsistent with an advection-dominated model for Sgr A\*, which assumes that the accretion rate is of order the canonical Bondi rate  $\sim 10^{-4}$  to  $10^{-5} M_\odot \text{ yr}^{-1}$ . We point out that strong rotation measure does not in principle limit densities and magnetic fields provided that the field has a very small bias superimposed on it, which is required to define the sign of circular polarization, and that the dispersion of the projected magnetic field on the sky is not too large. This implies that ‘high’ accretion rates comparable to the Bondi rate cannot be excluded on these grounds. More work on this issue is required to fully exploit the information contained in polarization observations in order to constrain physical conditions in Sgr A\*.

## 6.3. Radio galaxy M81\*

Brunthaler et al. (2001) detected circular polarization in the compact radio jet of the nearby spiral galaxy M81. Their estimated values of CP were  $0.27 \pm 0.06 \pm 0.07\%$  at 4.8 GHz and  $0.54 \pm 0.06 \pm 0.07\%$  at 8.4 GHz, where errors are separated into statistical and systematic terms. This suggests that the CP spectrum is flat or possibly inverted. They also detected no linear polarization at a level of 0.1%, indicating that the source has a high circular-to-linear polarization ratio. The spectral index indicates that this source is synchrotron thick and we can apply the same approach as for Sgr A\*. For example, for  $\xi \sim 50$  and  $\delta\zeta \sim 80$  we get a flat to slightly positive CP spectral index, CP/LP ratio  $\sim 4.7$  and  $\pi_c \sim 0.33\%$ .

#### 6.4. IDV blazar PKS 1519-273

Macquart et al. (2000) reported strongly variable circular and linear polarization from the intraday variable blazar PKS 1519-273. The source was characterized by an inverted intensity spectrum. The spectrum of circular polarization was roughly consistent with being flat or inverted (see their Fig. 3c) and typical values of linear and circular polarizations were a few percent and  $\sim 1\%$ , respectively. These data can be explained, for example, in the limit of high synchrotron depth. In order to have a roughly flat/inverted CP spectrum, we need the bias to correspond approximately to  $\delta$  near or below the extremum in circular polarization according to curves in Fig. 3. Levels of linear and circular polarization, in qualitative agreement with the observed ones, can be obtained for various combinations of  $\xi$  and the dispersion of the projected random magnetic field on the sky ( $2p-1$ ) (cf. equations [6]–[8] and see Figures 2 and 3). Alternatively, the data can be explained for synchrotron depth  $\tau \sim 1$ . In this case, the flatness of the synchrotron spectrum could be explained by means of a Blandford-Königl model in which the photospheric surface of constant, model-dependent, synchrotron depth moves outward along the jet with decreasing frequency. The required levels of CP and LP can then be obtained easily for the parameters considered in Fig. 5 (see middle and right panel).

#### 6.5. X-ray binary SS 433

Fender et al. (2000) detected circular polarization from the radio jet in the famous X-ray binary SS 433. The flux density spectra of circular polarization and Stokes  $I$  were roughly of the form  $V \propto I \propto \nu^{-1}$ . However, multiple components in the source and a lack of high spatial resolution prevented determination of the origin of circular polarization and the spectrum of fractional polarization. They argued that the CP emission is likely to be produced in the innermost regions of the binary, and that the fractional CP of this region can be as high as 10%. In this case the ratio of the fractional circular polarization to the overall linear polarization ( $\lesssim 1\%$ ) would exceed unity. If circular polarization originates from regions characterized by synchrotron depth  $\tau \gg 1$ , then the underlying synchrotron spectrum from this region would be approximately flat/inverted (Paragi et al. 1999). Then, the fractional CP spectrum would scale roughly  $\propto \nu^{-1}$ , which corresponds to a bias  $\delta$  (and mean rotativity) greater than that associated with the CP extremum. The highest circular polarization would then be about 3%. Note that in

such a situation we would also expect an excess of CP over LP even in the innermost regions of SS 433. If CP originates from the inner parts of the binary but from regions of  $\tau \lesssim 1$ , then the flatness of the synchrotron spectrum could be explained by means of a Blandford-Königl model. In such a scenario, the maximum fractional CP from the central regions could be as high as  $\sim 20\%$  (see Fig 4) and the CP spectrum could have a negative slope  $\beta$  ( $\pi_c \propto \nu^\beta$ ; cf. eq. [19] for  $\tau_\xi \ll 1$ ).

## 7. CONCLUSIONS

We have considered the transfer of polarized synchrotron radiation in stochastic sources by means of an analytic approach and a set of numerical simulations, and have argued that Faraday conversion is the primary mechanism responsible for the circular polarization properties of compact radio sources. A crucial ingredient of our model is a small bias in the highly turbulent magnetic field which accounts for the persistence of the sign of circular polarization. This bias is direct evidence for the net magnetic flux carried by magnetically accelerated jets (e.g., Blandford and Payne (1982); Li et al. (1992)).

Extremely large rates of Faraday rotation, i.e., Faraday rotation per unit synchrotron absorption depth, do not necessarily lead to depolarization provided that the mean rate of Faraday rotation across the source is relatively small, or in other words, that the turbulent magnetic field possesses a very small directional bias. Indeed, a large Faraday rotativity is required in order to explain the high ratio of circular to linear polarization observed in some sources. Constraints on jet composition or accretion rate, based on the requirement that the source does not become Faraday depolarized, may be circumvented under these conditions.

Gradients in Faraday rotation across turbulent cells can lead to correlations between rotativity and Stokes  $Q$  and  $U$  parameters, which can result in “correlation depolarization”. Observed polarization levels require that the field have many reversals along the line of sight to avoid this effect. Statistical fluctuations of circular and linear polarizations are then likely to be dominated by changes in the mean parameters describing the plasma rather than by the stochastic behavior of the turbulent medium. Variations in the mean parameters are unlikely to change the helicity of circular polarization unless a source undergoes a sharp transition from very low to very high synchrotron depth.

We have shown that our model is potentially applicable to a wide range of compact synchrotron sources. In particular, it naturally predicts an excess of circular over linear polarization when a source is strongly depolarized by the mean Faraday rotation and when a small amount of linear polarization is efficiently converted into circular polarization. This can explain the polarization properties of the Galactic Center and M81\*.

We thank Roger Blandford, Avery Broderick and Marek Sikora for insightful discussions. This work was supported in part by NSF grant AST-9876887.

## APPENDIX

## TRANSFER OF POLARIZED RADIATION

The transfer equation of polarized radiation reads (Zheleznyakov et al. 1974; Jones 1988)<sup>3</sup>:

$$\begin{pmatrix} \left(\frac{d}{d\tau} + 1\right) & \zeta_q \cos 2\phi & -\zeta_q \sin 2\phi & \zeta_v \\ \zeta_q \cos 2\phi & \left(\frac{d}{d\tau} + 1\right) & \zeta_v^* & \zeta_q^* \sin 2\phi \\ -\zeta_q \sin 2\phi & -\zeta_v^* & \left(\frac{d}{d\tau} + 1\right) & \zeta_q^* \cos 2\phi \\ \zeta_v & -\zeta_q^* \sin 2\phi & -\zeta_q^* \cos 2\phi & \left(\frac{d}{d\tau} + 1\right) \end{pmatrix} \begin{pmatrix} I \\ Q \\ U \\ V \end{pmatrix} = \begin{pmatrix} 1 \\ \epsilon_q \cos 2\phi \\ -\epsilon_q \sin 2\phi \\ \epsilon_v \end{pmatrix} J \quad (A1)$$

where  $I$ ,  $Q$ ,  $U$  and  $V$  are the usual Stokes parameters,  $\tau \propto (\nu_B/\nu)^{\alpha+5/2} \nu_B^{-1}$  is the synchrotron optical depth,  $J$  is the source function,  $\phi$  is the azimuthal projection angle of the magnetic field on the sky and the coefficients of emissivity ( $\epsilon_q$ ,  $\epsilon_v$ ), absorptivity ( $\zeta_q$ ,  $\zeta_v$ ), convertibility ( $\zeta_q^*$ ) and rotativity ( $\zeta_v^*$ ) are given by:

$$\epsilon_q = \epsilon_\alpha^q \quad (A2)$$

$$\epsilon_v = 0 \quad (A3)$$

$$\zeta_q = \zeta_\alpha^q \quad (A4)$$

$$\zeta_v = 0 \quad (A5)$$

$$\zeta_q^* = - \left( 1 + \frac{\zeta_q^{*(c)}}{\zeta_q^{*(r)}} \right) \zeta_\alpha^{*q} \left( \frac{\nu_B}{\nu} \right)^{\alpha-1/2} \left[ 1 - \left( \frac{\nu_i}{\nu} \right)^{\alpha-1/2} \right] \left( \alpha - \frac{1}{2} \right)^{-1}, \quad \alpha > \frac{1}{2} \quad (A6)$$

$$\zeta_v^* = \left( 1 + \frac{\zeta_v^{*(c)}}{\zeta_v^{*(r)}} \right) \zeta_\alpha^{*v} \left( \frac{\nu}{\nu_i} \right)^{\alpha+1/2} \frac{\ln \gamma_i}{\gamma_i} \left( \frac{n_r^- - n_r^+}{n_r^- + n_r^+} \right) \cot \theta \quad (A7)$$

where  $\zeta_{v,q}^{*(c)}/\zeta_{v,q}^{*(r)}$  are the ratios of convertibilities ( $q$ ) and rotativities ( $v$ ) of the cold ( $c$ ) and relativistic ( $r$ ) plasmas given by:

$$\frac{\zeta_q^{*(c)}}{\zeta_q^{*(r)}} = \frac{1}{2\alpha} \frac{\alpha - 1/2}{1 - (\nu/\nu_i)^{\alpha-1/2}} \frac{1}{\gamma_i} \frac{n_c^- + n_c^+}{n_r^- + n_r^+} \quad (A8)$$

$$\frac{\zeta_v^{*(c)}}{\zeta_v^{*(r)}} = \frac{1}{2\alpha} \frac{\alpha + 1}{\alpha + 3/2} \frac{\gamma_i^2}{\ln \gamma_i} \frac{n_c^- - n_c^+}{n_r^- - n_r^+}. \quad (A9)$$

The transfer coefficients have been generalized to include contributions from both electron and positron plasmas but they assume an isotropic pitch-angle distribution of the radiating particles. We also neglected circular emissivity  $\epsilon_v$  and absorptivity  $\zeta_v$  (Jones and O'Dell 1977a). In the above equations,  $n_{c,r}^{+,-}$  are number densities of cold/relativistic electrons ( $-$ ) or positrons ( $+$ ),  $\nu_B = eB \sin \theta / 2\pi m_e c$  is the Larmor frequency,  $\gamma_i$  is the low-energy cut-off Lorentz factor of relativistic particles,  $\nu_i = \gamma_i^2 \nu_B$  is the frequency corresponding to radiating particles of energy  $\sim \gamma_i m_e c^2$ ,  $\alpha$  is the synchrotron-thin spectral index which also defines the slope of the relativistic particle energy distribution  $n(\gamma) \propto \gamma^{-2\alpha-1}$ ,  $\theta$  is the angle between the line of sight and the direction of the magnetic field and  $\epsilon_\alpha^q$ ,  $\zeta_\alpha^q$ ,  $\zeta_\alpha^{*q}$  and  $\zeta_\alpha^{*v}$  are the proportionality coefficients which are tabulated in Jones and O'Dell (1977a).

We integrated the radiative transfer equations using the Cash-Karp embedded Runge-Kutta fifth-order method with an adaptive stepsize control (Press et al. 1992). Computations were performed by integrating transfer equations in a piece-wise homogeneous medium. The physical conditions in each cell, i.e., orientation of the magnetic field vector, were chosen using the random number generation method of L'Ecuyer in the implementation provided by Press et al. (1992). This method is particularly suited for our purposes as it generates long-period sequences of random numbers and thus prevents any spurious correlations. We assumed a constant strength of the variable  $\mathbf{B}$ -field component but allowed its solid angle distribution to be uniform within  $\theta \in (0^\circ, 180^\circ)$  and  $\phi \in (-\phi_o, \phi_o)$ , where  $\langle \cos 2\phi \rangle_{(-\phi_o, \phi_o)} = 2p - 1$  is the average of  $\cos 2\phi$  in the interval  $(-\phi_o, \phi_o)$ . We also superimposed a weak constant and unidirectional component  $|\mathbf{B}_u| = \delta |\mathbf{B}|$  on the variable magnetic field.

<sup>3</sup> Our formulae are free from typographic errors found in Jones (1988).

## REFERENCES

Agol, E. 2000, ApJ, 538, L121

Aitken, D.K., Greaves, J., Chrysostomou, A., Jennes, T., Holland, W., Hough, J.H., Pierce-Price, D., and Richer J. 2000, ApJ, 534, L173

Begelman, M.C., Blandford R.D., and Rees, M.J. 1984, Rev. Mod. Phys., 56, 255

Benford, G., and Tzach, D. 2000, MNRAS, 317, 497

Björnsson, C.-I. 1990, MNRAS, 242, 158

Blandford, R.D., and Königl, A. 1979, ApJ, 232, 34

Blandford, R.D., and Payne, D.G. 1982, MNRAS, 199, 883

Bower, G.C. 2000, GCNEWS, 11, 4, <http://www.mpiifr-bonn.mpg.de/gcnews/index.shtml>

Bower, G.C., Falcke, H., and Backer, D.C. 1999, ApJ, 523, L29

Bower, G.C., Falcke, H., Sault, H., and Backer, D.C. 2000, in preparation

Brunthaler, A., Bower, G.C., Falcke, H., and Mellon, R.R. 2001, ApJL, in press, astro-ph/0109170

Dieckmann, M.E., Chapman, S.C., McClements K.G., Dendy, R.O., and Drury, L.O'C. 2000, A&A, 356, 377

Eckart, A., and Genzel, R. 1996, Nature, 383, 415

Eckart, A., and Genzel, R. 1997, MNRAS, 284, 776

Fender, R., Rayner D., Norris R., Sault R.J., and Pooley, G. 2000, ApJ, 530, L29

Fuki, A.A., Kravtsov, Yu.A., and Naida, O.N. 1998, *Geometrical Optics of Weakly Anisotropic Media* (Gordon & Breach)

Ghez, A., Klein, B.L., Morris, M., and Becklin, E.E. 1998, ApJ, 509, 678

Ginzburg, V.L. 1961, *The Propagation of Electromagnetic Waves in Plasma* (New York: Gordon & Breach)

Homan, D.C., and Wardle, J.F.C. 1999, AJ, 118, 1942

Homan, D.C., Attridge, J.M., and Wardle J.F.C. 2001, ApJ, 556, 113

Hughes, P.A., Aller H.D., and Aller M.F. 1989, ApJ, 341, 54

Jones, T.W. 1988, ApJ, 332, 678

Jones, T.W., and O'Dell S.L. 1977, ApJ, 214, 522

Jones, T.W., and O'Dell S.L. 1977, ApJ, 215, 236

Jones, T.W., Rudnick, L., Aller, H.D., Aller, M.F., Hodge, P.E., and Fiedler, R.L. 1985, ApJ, 290, 627

Kennet, M., Melrose, D. 1998, PASA, 15, 211

Komesaroff, M.M., Roberts, J.A., Milne, D.K., Rayner, P.T., and Cooke, D.J. 1984, MNRAS, 208, 409

Laing, R.A. 1980, MNRAS, 193, 493

Laing, R.A. 1981, ApJ, 248, 87

Legg, M.P.C., and Westfold, K.C. 1968, ApJ, 154, 499

Li Z-Y., Chiueh, T., and Begelman M.C. 1992, ApJ, 394, 459

Macquart, J.-P., and Melrose, D.B. 2000, ApJ, 545, 798

Macquart, J.-P., Kedziora-Chudczer, L., Rayner, D.P., and Jauncey, D.L. 2000, ApJ, 538, 623

Melia, F., and Falcke, H. 2001, ARA&A, 39, 309

Melrose D.B., and McPadden, R.C. 1991, *Electromagnetic processes in dispersive media : A treatment based on the dielectric tensor*, Cambridge [England] ; New York : Cambridge University Press

Marscher, A.P., and Gear, W.K. 1985, ApJ, 298, 114

Noerdlinger, P.D. 1978, Phy. Rev. Lett, 41, 135

Pacholczyk, A.G., and Swihart, T.L. 1975, ApJ, 197, 125

Paragi, Z., Vermeulen, R.C., Fejes, I., Schilizzi, R.T., Spencer, R.E., and Stirling, A.M. 1999, A&A, 348, 910

Press, W.H., Teukolsky, S.A., Vetterling, W.T., and Flannery, B.P. 1992, *Numerical Recipes in C: The art of scientific computing*, Cambridge [England] ; Cambridge University Press

Quataert, E., and Gruzinov, A. 2000, ApJ, 545, 842

Rayner, D.P., Norris, R.P., and Sault, R.J. 2000, MNRAS, 319, 484

Readhead, A.C.S. 1994, ApJ, 426, 51

Rusk, R.E., and Seaquist, E.R. 1985, J.R.A.S. Canada, 79, 246

Sault, R.J., and Macquart, J.-P. 1999, ApJ, 526, L85

Sazonov, V.N. 1969, Sov. Phys. JETP, 29, 578

Shimada, N., and Hoshino, M. 2000, ApJ, 543, L67

Sikora M., and Madejski G. 2000, ApJ, 534, 109

Thompson, C., Blandford, R.D., Evans, C.R., and Phinney, E.S. 1994, ApJ, 422, 304

Wardle, J.F.C., and Roberts D.H. 1994, in *Compact Extragalactic Radio Sources* (eds Zensus, J.A., and Kellerman, K.I.), 217, (Workshop Proc., NRAO, Socorro, NM)

Wardle, J.F.C., Homan, D.C., Ojha, R., and Roberts, D.H. 1998, Nature, 395, 457

Weiler, K.W., and de Pater, I. 1983, ApJS, 52, 293

Zheleznyakov, V.V., Suvorov, E.V., and Shaposhnikov, V.E. 1974, Soviet Astr.-AJ, 18, 142

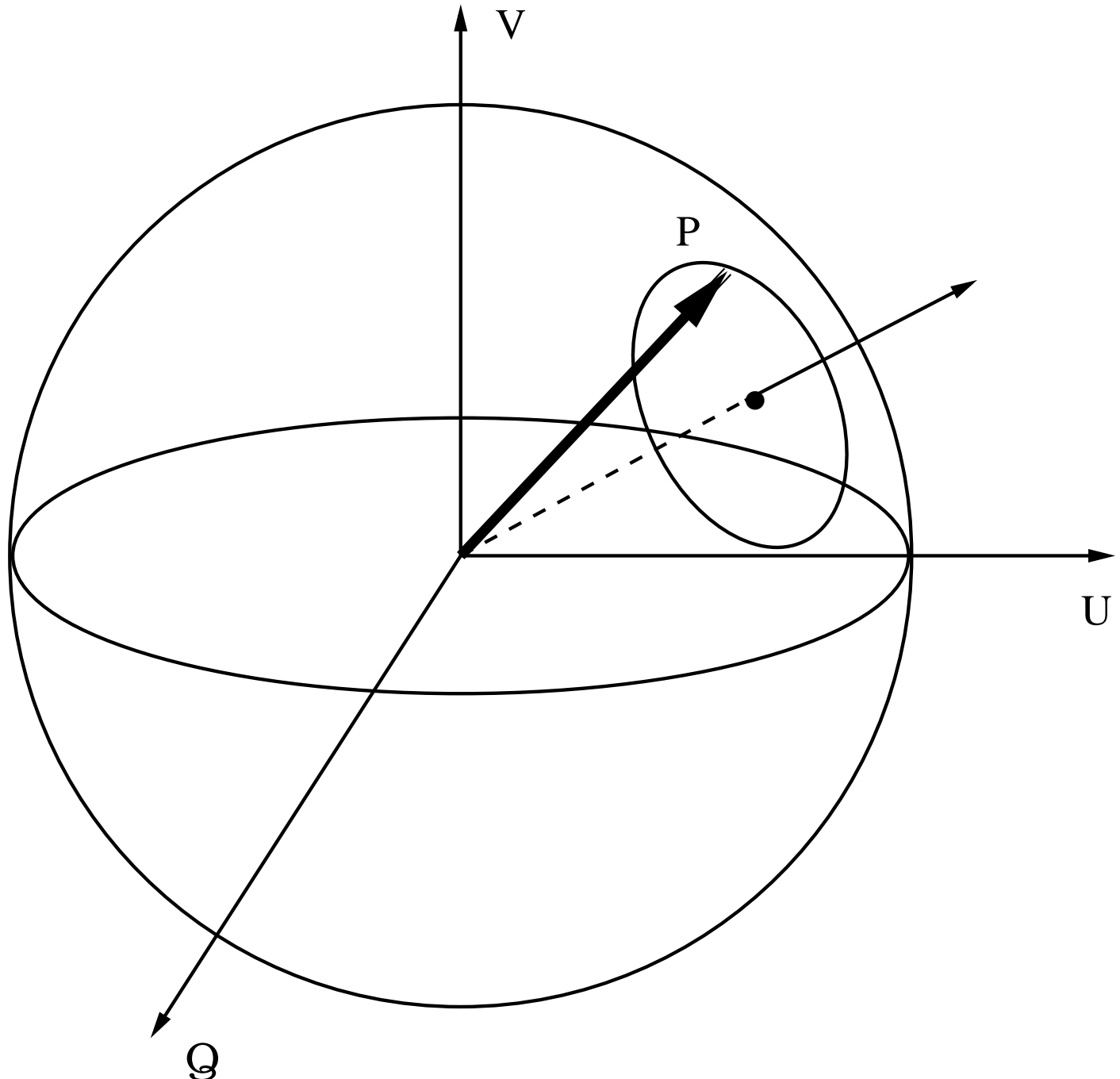


FIG. A1.— The Poincaré sphere with the natural mode axis (dashed line) and the polarization vector  $\mathbf{P}$  (thick solid line). Circular and linear polarizations correspond to the poles and the equator, respectively.

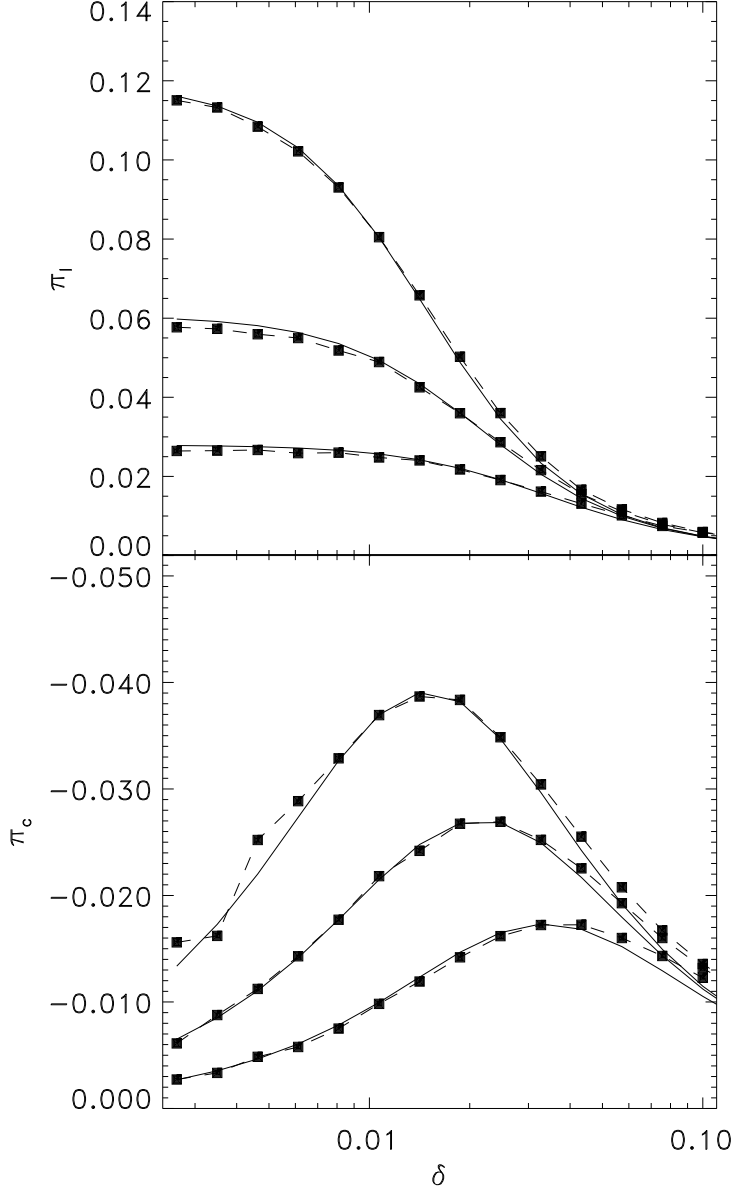


FIG. A2.— Linear (upper panel) and circular polarizations for high synchrotron depth ( $\tau_0 \approx 27$ ) and varying number of turbulent zones along the line of sight ( $N = 10^8, 3 \times 10^5$  and  $10^5$ ; from top to bottom, respectively). Other parameters used in this simulation were:  $\alpha = 0.5$ ,  $\gamma_i = 3$ ,  $\gamma = 50$ ,  $p = 1$  and  $\theta_u = 45^\circ$ . Solid lines denote analytical results and squares connected by dashed lines denote results of Monte Carlo simulations.

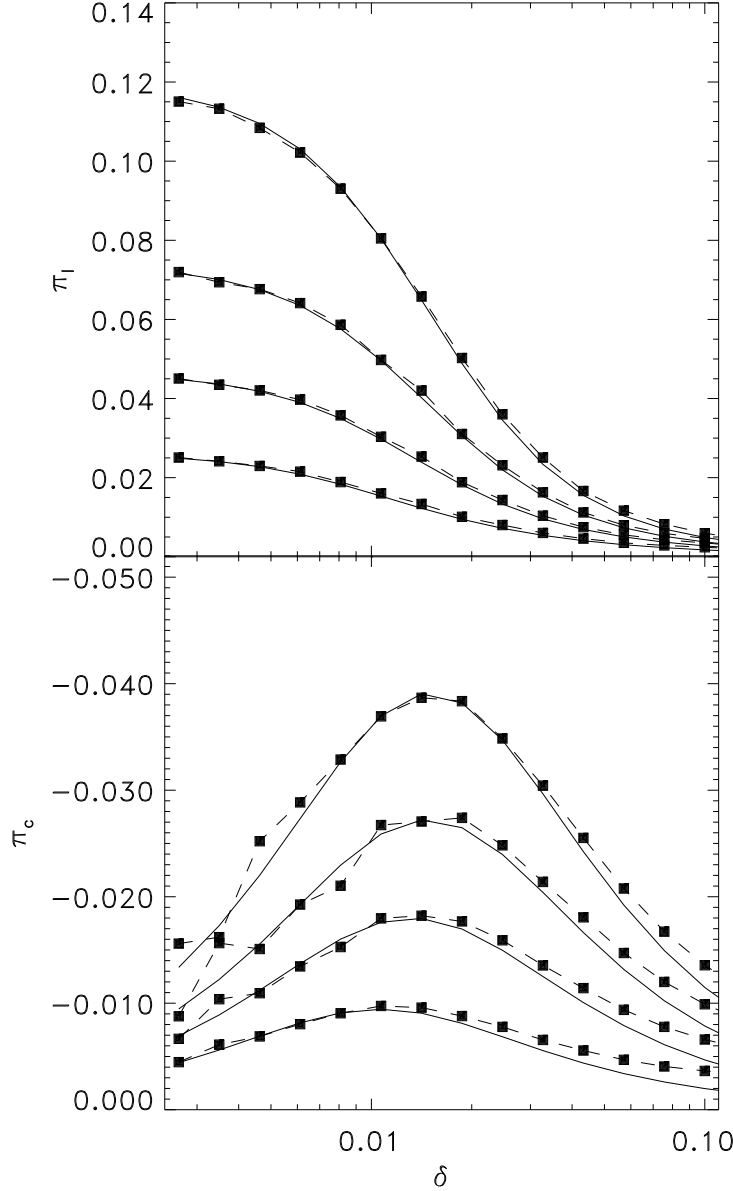


FIG. A3.— Linear (upper panel) and circular polarizations for high synchrotron depth, large number of field reversals along the line of sight ('saturated' polarization) and varying dispersion of the projected turbulent magnetic field on the plane of the sky ( $\phi$  is distributed uniformly in  $[-\Delta\phi, \Delta\phi]$ ;  $\Delta\phi = 0^\circ$  ( $p = 1$ ),  $\Delta\phi = 30^\circ$  ( $p = 0.91$ ),  $\Delta\phi = 45^\circ$  ( $p = 0.82$ ),  $\Delta\phi = 60^\circ$  ( $p = 0.71$ ); from top to bottom, respectively. Other parameters used in this simulation were:  $\alpha = 0.5$ ,  $\gamma_i = 3$ ,  $\gamma = 50$  and  $\theta_u = 45^\circ$ . Solid lines denote analytical results and squares connected by dashed lines denote results of Monte Carlo simulations.

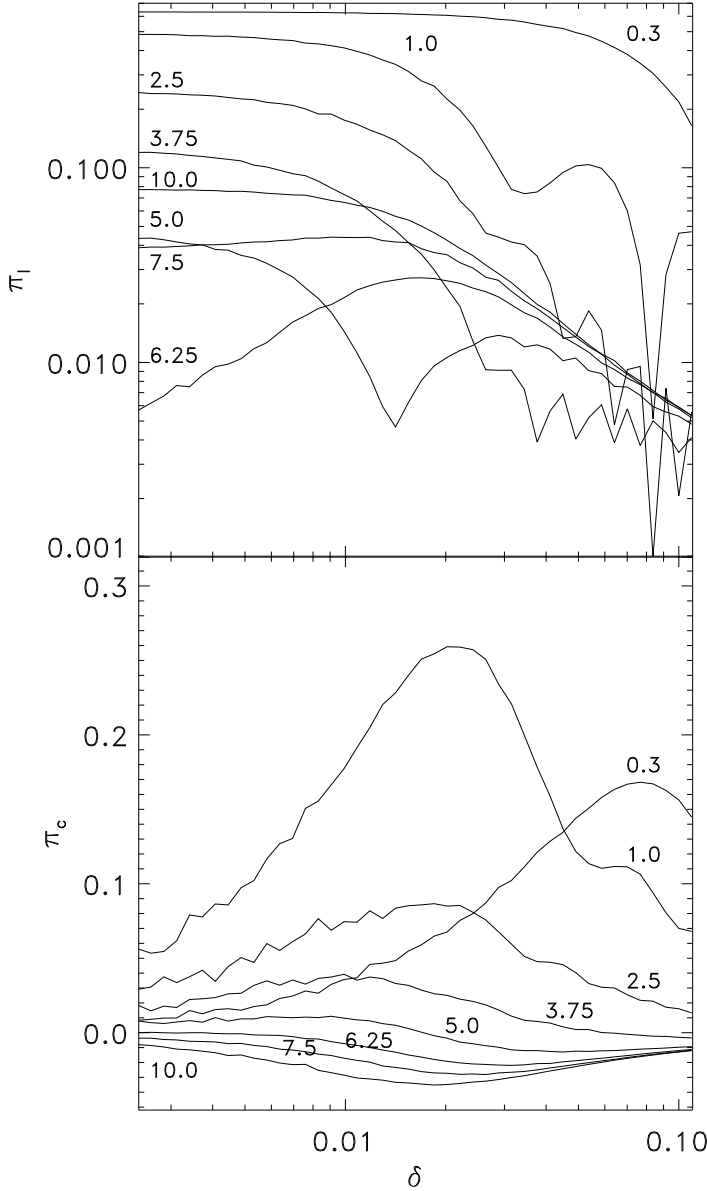


FIG. A4.— Linear (upper panel) and circular polarizations (lower panel) for a large number of field reversals along the line of sight ('saturated' polarization) and varying maximum synchrotron depth. Each curve is labeled with the value of the synchrotron depth. Other parameters used in this simulation were:  $\alpha = 0.5$ ,  $\gamma_i = 3$ ,  $\gamma = 50$ ,  $p = 1$  and  $\theta_u = 45^\circ$ .

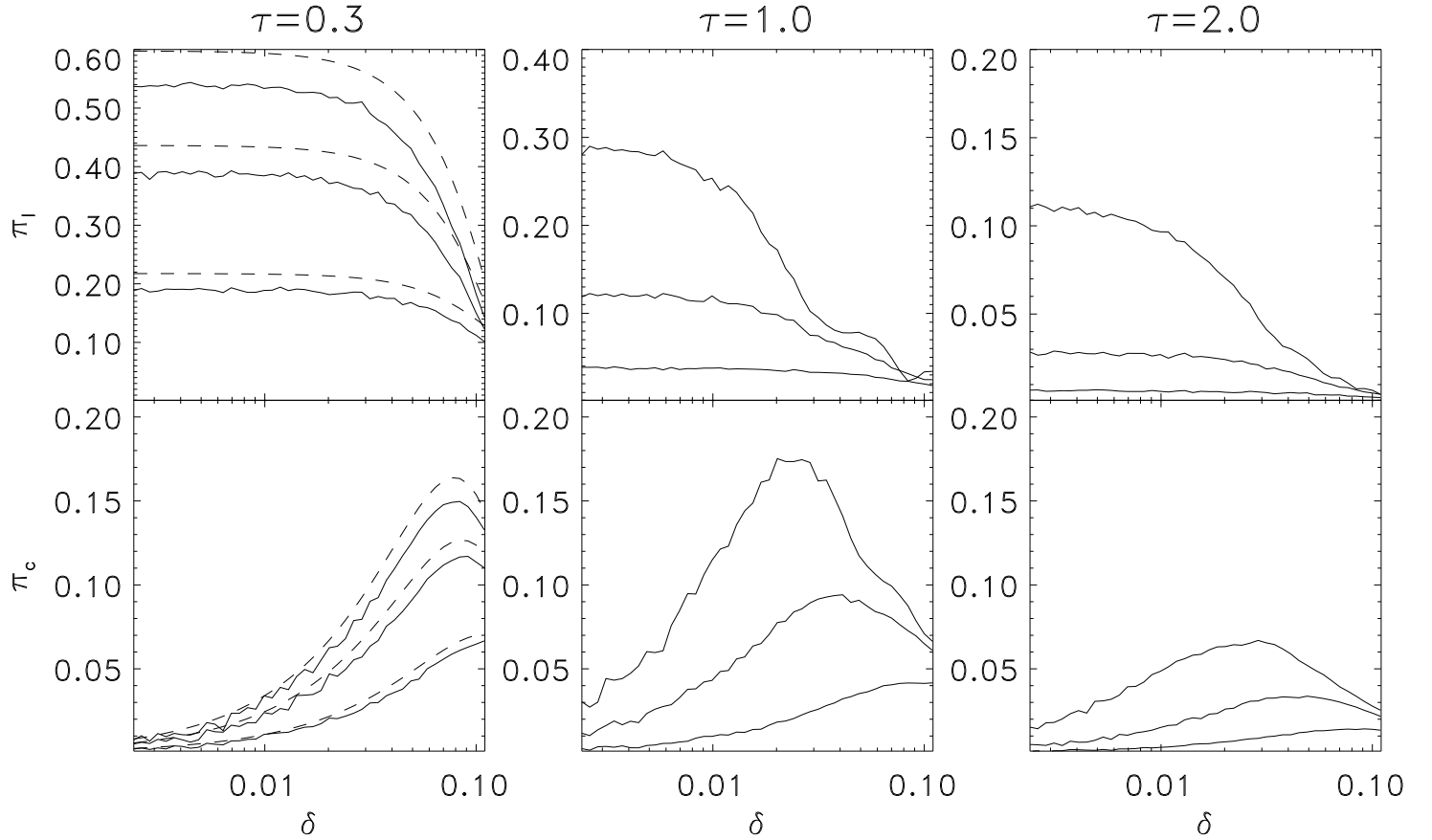


FIG. A5.— Linear (upper panels) and circular polarizations (lower panels) for moderate values of synchrotron depth (top labels) and different numbers of turbulent cells  $N$  along the line of sight. The curves correspond to  $N = 187$ ,  $N = 562$  and  $N = 1875$  (left panel; from bottom to top, respectively),  $N = 625$ ,  $N = 1875$  and  $N = 6250$  (middle panel; from bottom to top, respectively) and  $N = 1250$ ,  $N = 3750$  and  $N = 12500$  (right panel; from bottom to top, respectively). Other parameters used in this simulation were:  $\alpha = 0.5$ ,  $\gamma_i = 3$ ,  $\gamma = 50$ ,  $p = 1$  and  $\theta_u = 45^\circ$ . Dashed lines on the left panel are the analytical results for small synchrotron depth.